HYDROLOGICAL PROCESSES
Hydrol. Process. **28**, 2324–2337 (2014)
Published online 4 April 2013 in Wiley Online Library
(wileyonlinelibrary.com) DOI: 10.1002/hyp.9778

Temporal and spatial response of hyporheic zone geochemistry to a storm event

Margaret A. Zimmer* and Laura K. Lautz

Department of Earth Sciences, Syracuse University, Syracuse, NY, USA

Abstract:

Although there has been recent focus on understanding spatial variability in hyporheic zone geochemistry across different morphological units under baseflow conditions, less attention has been paid to temporal responses of hyporheic zone geochemistry to non-steady-state conditions. We documented spatial and temporal variability of hyporheic zone geochemistry in response to a large-scale storm event, Tropical Storm Irene (August 2011), across a pool–riffle–pool sequence along Chittenango Creek in Chittenango, NY, USA. We sampled stream water as well as pore water at 15 cm depth in the streambed at 14 locations across a 30 m reach. Sampling occurred seven times at daily intervals: once during baseflow conditions, once during the rising limb of the storm hydrograph, and five times during the receding limb. Principal component analysis was used to interpret temporal and spatial changes and dominant drivers in stream and pore water geochemistry ($n = 111$). Results show the majority of spatial variance in hyporheic geochemistry (62%) is driven by differential mixing of stream and ground water in the hyporheic zone. The second largest driver (17%) of hyporheic geochemistry was temporal dilution and enrichment of infiltrating stream water during the storm. Hyporheic sites minimally influenced by discharging groundwater ('connected' sites) showed temporal changes in water chemistry in response to the storm event. Connected sites within and upstream of the riffle reflected stream geochemistry throughout the storm, whereas downstream sites showed temporally lagged responses in some conservative and biogeochemically reactive solutes. This suggests temporal changes in hyporheic geochemistry at these locations reflect a combination of changes in infiltrating stream chemistry and hyporheic flowpath length and residence time. The portion of the study area strongly influenced by groundwater discharge increased in size throughout the storm, producing elevated Ca^{2+} and SO_4^{2-} concentrations in the streambed, suggesting zones of localized groundwater inputs expand in response to storms.

KEY WORDS hyporheic zone; storm event; surface water-groundwater interactions; principal component analysis; streambed

Received 8 June 2012; Accepted 19 February 2013

INTRODUCTION

The hyporheic zone marks the dynamic ecotone where stream water interacts with the surrounding subsurface aquifer, allowing for mixing with groundwater (Hayashi and Rosenberry, 2002). Hyporheic exchange is the process by which water from the stream infiltrates into the hyporheic zone, in either the streambed or the adjacent stream banks, and returns to the stream over small distances or time (Harvey *et al*., 1996; Gooseff, 2010). Hyporheic exchange, which is influenced by stream discharge, hydraulic conductivity, and channel morphology (Wroblicky *et al*., 1998; Harvey and Wagner, 2000; Storey *et al*., 2003), can transport, retain, and transform nutrients and oxygen and contribute to unique benthic and riparian habitats (Boulton *et al*., 1998).

Recent model and field experiments on stream–groundwater interactions have focused largely on understanding how bedform topography produces predictable zones of hyporheic exchange during steady-state conditions (e.g. Kasahara and Wondzell, 2003; Kasahara and Hill, 2006; Cardenas and Wilson, 2007; Fanelli and Lautz, 2008; Hester and Doyle, 2008; Wondzell, 2011; Briggs *et al*., 2012). Kasahara and Hill (2006) showed that during baseflow conditions in riffle bedforms, there are zones of surface water downwelling immediately upstream of riffle bedforms, which produce oxic streambed conditions. They showed zones of groundwater upwelling occur immediately downstream of riffle bedforms, which produce anoxic streambed conditions. This predictable spatial patchiness drives the development of micro-environments throughout the streambed, by providing variable amounts of dissolved oxygen, nutrients, and organic matter across the system (Valett *et al*., 1994; Hayashi and Rosenberry, 2002; Boulton, 2007). However, it is unclear how this spatial patchiness around riffle bedforms persists during, or responds to, periods of non-baseflow conditions.

Most annual watershed export of solutes occurs during storms (Inamdar *et al*., 2004; Creed and Band, 1998). However, the geochemical role and response of the hyporheic zone to storms is currently poorly understood (Wondzell, 2011). On the basis of a literature review described in the following paragraphs, there are currently two main physical processes thought to control hyporheic exchange during periods of fluctuating stream stage, such as storms. The first process is the increase in hydraulic head at the streambed interface as stream stage increases,

*Correspondence to: Margaret A. Zimmer, Department of Earth Sciences, Syracuse University, 204 Heroy Geology Lab, Syracuse, NY 13244, USA.
E-mail: mazimm02@syr.edu

which causes a rapid influx of stream water into the hyporheic zone. The second process is the increase in the hydraulic gradient towards the stream, resulting from storm water recharge to the adjacent groundwater aquifer, which causes the size of the hyporheic zone to decrease.

The majority of studies that have investigated the increase in hyporheic exchange in response to rising stream stage (i.e. the first process described earlier) are field studies that focus on measurements within the stream channel at relatively shallow depths, have no precipitation input, and largely ignore adjacent aquifer dynamics (e.g. D'Angelo *et al*., 1993; Arntzen *et al*., 2006; Sawyer *et al*., 2009; Briggs *et al*., 2012). Gerecht *et al*. (2011) showed that hyporheic exchange went from upwelling to downwelling with an increase in stream stage during a dam storage–release cycle. Similarly, Fritz and Arntzen (2007) and Francis *et al*. (2010) saw a positive correlation between artificial fluctuations in stream stage and hyporheic exchange in field studies around regulated dam spillways. Further, some modelling studies that focused analysis on the stream and ignored groundwater upwelling (Boano *et al*., 2007; Boano *et al*., 2010) showed an increase in exchange rates with increasing stream stage.

Studies that have investigated the decrease in hyporheic zone size during storm events (i.e. the second process described earlier) are primarily modelling studies that take into account groundwater dynamics in the surrounding aquifer (e.g. Harvey and Bencala, 1993; Wroblicky *et al*., 1998; Storey *et al*., 2003). Wondzell and Swanson (1996) used a MODFLOW model to show that subsurface flow rates to a gravel bar adjacent to a fourth-order stream positively correlate to stream discharge during baseflow conditions but decrease during storm events because of precipitation inputs to the aquifer. Shibata *et al*. (2004) also used MODFLOW to demonstrate that contributions of soil water to the stream from the adjacent hillslope increase during storm events, whereas stream water contributions to the adjacent aquifer decrease. Boano *et al*. (2008) modelled that an increase in groundwater levels in the adjacent aquifer altered hyporheic exchange rates across the stream channel differently, on the basis of lateral distance from the aquifer. They showed exchange rates were reduced along the banks and the majority of hyporheic exchange was confined to the central part of the stream, where upwelling groundwater flowpaths from the adjacent aquifer were not as influential.

Some studies that have used both streambed and adjacent aquifer analyses to investigate hyporheic response to changing stream stage have shown the influence of both processes during storm events. A field study by Morrice *et al*. (1997) showed that a seasonal increase in stream discharge and hydraulic gradients towards the stream from a seasonal rise in the water table increased the rate of hyporheic exchange, but reduced the size of the hyporheic zone. Similarly, Hart *et al*. (1999) showed in a field study that storage zone size did not change in response to variations in flow conditions, but rates of exchange increased because of increasing stream discharge. Malcolm *et al*. (2004) saw in a field study that on a weekly scale, low flow conditions promoted groundwater contributions to the hyporheic zone and higher flow conditions promoted increased surface water contributions to the hyporheic zone. Malcolm *et al*. (2004) further showed that during storm events, high-resolution hydraulic head data in the centre of a riffle bedform indicated that the stream went from slightly gaining to losing during the rising limb of storm hydrographs. Upward gradients were re-established late into the receding limb of the storm hydrograph. Westhoff *et al*. (2011) examined groundwater and stream water inputs throughout the hyporheic zone during a small precipitation event and saw an increase in stream water infiltration to the streambed but no change in groundwater inputs.

The majority of field studies on hyporheic zone response to variable stream discharge examine how hyporheic exchange responds to seasonal changes in stream stage (e.g. Wondzell and Swanson, 1996; Morrice *et al*., 1997; Hart *et al*., 1999; Malcolm *et al*., 2004; Briggs *et al*., 2012) or dam-regulated stream flow (e.g. Fritz and Arntzen, 2007; Francis *et al*., 2010, Gerecht *et al*., 2011) or how hyporheic exchange varies between streams with different magnitudes of discharge (e.g. D'Angelo *et al*., 1993). Fewer studies examine hyporheic exchange responses to storm events (e.g. Wondzell and Swanson, 1996; Malcolm *et al*., 2004, 2006); however, most of these studies predominantly focus on physical hydrology and not geochemical changes. Our study addresses the gap in knowledge regarding how stream–groundwater exchange rates and streambed geochemistry respond to a rapid fluctuation in stream stage, such as during a large-scale storm event. To address this gap in knowledge, we measured spatial and temporal changes in surface water and pore water solute concentrations in a 30 m reach of a stream during a large storm event, specifically Tropical Storm Irene in August 2011. The objectives of this study were to (1) characterize spatial vertical water exchange rates and geochemical patterns in the hyporheic zone around a pool–riffle–pool bedform during baseflow and (2) use results from principal component analyses (PCA) and time-series geochemical analyses to conceptualize how different regions of the hyporheic zone respond to storm events.

METHODS

Site description

This study was conducted along a 30 m stream reach of Chittenango Creek (Figure 1), an ungauged tributary to Oneida Lake, near Syracuse, NY, USA (43°00′ 32.27″ N 75°50′ 49.85″ W, elevation ~178 m). The drainage area to Chittenango Creek is 750 km^2. The study reach parallels State Highway 13 and is downstream of Chittenango Falls, a 51-m waterfall. The study reach is a pool–riffle–pool sequence, and the streambed is composed of coarse sand and gravel. An acoustic Doppler velocimeter measurement of discharge calculated 0.80 m^3/s at the study reach during the August baseflow survey.

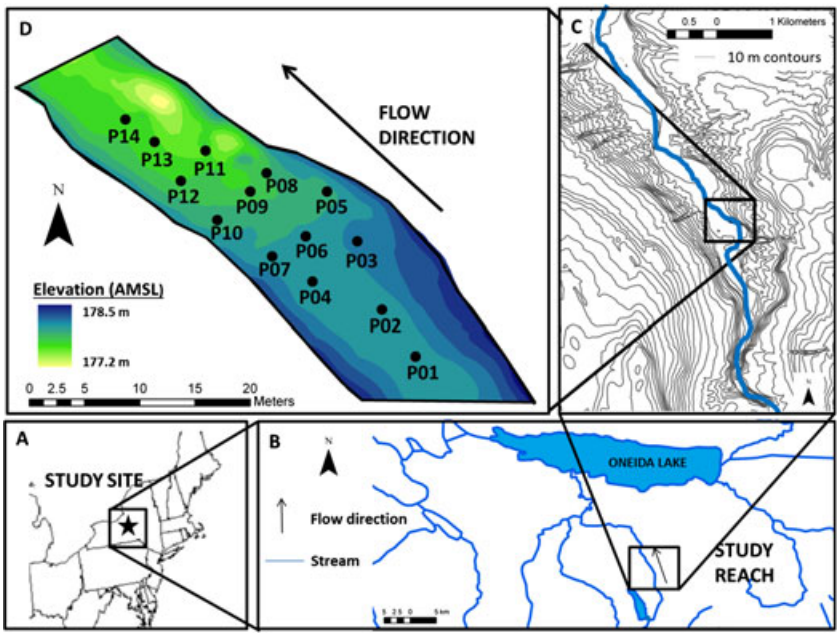

Figure 1. (A) Map of the study site and its location in central New York. (B) Map of Chittenango Creek watershed draining into Oneida Lake. (C) Map of elevation contours around the study reach. (D) Map of study reach. Labelled black points indicate coupled installation locations for mini-piezometers and temperature profile rods. Direction of stream water flow is shown with black arrow and colour shading on site map indicates streambed elevation, with blue values corresponding to higher elevations.

Precipitation and hydrograph information

The recurrence interval of Tropical Storm Irene at our study site was a 2- to 5-year storm, as interpreted by data provided by the Northeast Regional Climate Center and Natural Resources Conservation Service (http://precip.eas.cornell.edu). Because of the short-range forecast limiting preparation time, as well as safety considerations of collecting data during Tropical Storm Irene, precipitation and stream discharge measurements from the National Oceanic and Atmospheric Administration (NOAA) and United States Geological Survey (USGS) stations in central New York were used as a proxy for the conditions at our specific site. Daily precipitation data used for this study were collected in the town of Chittenango (Station ID: US1NYMD0016) by the National Climatic Data Center within NOAA. Approximately 6.2 cm of precipitation were measured at this station during the storm. Hydrographs were created from hourly discharge measurements taken at several regional USGS stations, all less than 55 km from the study site, including Oneida Creek at Oneida, NY (04243500); East Branch Fish Creek at Taberg, NY (04242500); and Otselic River at Cincinnatus, NY (01510000). We chose these three sites as they were geographically close to the study site and were relatively similar, albeit smaller, in contributing area. Discharge at each site was normalized to the highest discharge value during the study period in order to compare timing of peak discharge and storm flow recession. The discharge at the end of the study period was, on average, 25% greater than pre-event discharge at the three gauging stations.

Streambed instrumentation and storm sampling

To evaluate the topographic controls on stream and streambed interaction, we surveyed the morphology of the study site with a Nikon Nivo 5.M total station, which has a spatial resolution of <1 cm. We collected spatial information at 167 survey points to characterize bedform morphology, water elevation, water edge, and position of installed sampling equipment during baseflow conditions (Figure 1).

Temperature profile rods were coupled with mini-piezometers at 14 locations across the 30 m stream reach (Figure 1). Temperature profile rods contained seven vertically stacked temperature sensors (iButton DS1922L, Maxim Integrated, San Jose, CA, USA), with six installed in the streambed at 5-cm intervals to a depth of 30 cm and one positioned in the water column (depth = 0 cm). The temperature sensors recorded temperature at 10-min intervals for 7 days prior to the storm. Vertical water exchange rates at each location were calculated for baseflow conditions prior to the storm event using one-dimensional heat transport modelling (Hatch *et al.*, 2006; Gordon *et al.*, 2012). We used VFLUX (Gordon *et al.*, 2012), a MATLAB computer program, which derives exchange rates every 2 h during the observation period from the difference in amplitude of the propagated diurnal temperature signal measured at multiple depths (Hatch *et al.*, 2006). Exchange rates were calculated at depths of 2.5 and 5.0 cm using the 0- to 5-cm and 0- to 10-cm pairs of sensors, respectively. Two-hour exchange rates at both depths were averaged over the 7-day baseflow observation period to derive a single vertical exchange rate across the streambed interface for each observation point.

Mini-piezometers were constructed of PVC pipe (1.27 cm ID) with a 5-cm screen created by drilling a series of 0.3-cm diameter holes in the pipe. These mini-piezometers were installed 17.5 cm below the stream–streambed interface, such that the 5-cm screen was centred at 15 cm. Plastic tubing and a syringe were used to purge and sample pore water from the piezometers. At four of the 14 mini-piezometer locations (P02, P05, P07, and P11), we installed nested piezometers to determine how bed chemistry varies

with streambed depth. At P02 and P11, we installed mini-piezometers at 32.5 cm in addition to the standard depth of 17.5 cm. At P05 and P07, we installed mini-piezometers at 27.5 and 32.5 cm in addition to the standard depth of 17.5 cm.

Stream water as well as pore water from the mini-piezometers were sampled seven times throughout the study period. Of the seven sampling times, one baseflow sampling occurred on 27 August 2011, one sampling occurred during the rising limb of Tropical Storm Irene on 28 August 2011, and five samplings occurred once daily during the receding limb of the storm hydrograph from 30 August to 3 September 2011. There is a 2-day gap of no sampling during the peak portion of the stream hydrograph (28 and 29 August 2011) because of high flows limiting safe accessibility to the stream and sampling locations.

Samples were collected within a 2-h period on each sample date and were filtered with a 0.7 μM glass microfiber filter within an 8-h period. Specific conductance (SC), pH, and dissolved oxygen (DO) were measured in the field. Dissolved metals, specifically calcium (Ca^{2+}), sodium (Na^{+}), magnesium (Mg^{2+}), ammonium (NH_4^{+}), and potassium (K^{+}), as well as anions, specifically fluoride (F^{-}), bromide (Br^{-}), phosphate (PO_4^{3-}), chloride (Cl^{-}), nitrate (NO_3^{-}) and sulfate (SO_4^{2-}), were analysed on a Dionex ICS-2000 Ion Chromatograph. For this study, NH_4^{+}, Br^{-}, and PO_4^{3-} were not used because most samples registered below the detection limit.

Multivariate statistical analysis

Principal component analysis is a statistical tool used to summarize covariance between variables in large datasets by creating linear combinations of the original variables. Several recent studies have used PCA to summarize the variability of stream–groundwater interactions (Lautz and Fanelli, 2008; Lewandowski *et al*., 2009; Guggenmos *et al*., 2011).

In our study, we used the PRINCOMP method in the computer program MATLAB to run a PCA to interpret the relationships between solutes across the entire spatial and temporal stream and streambed geochemical dataset. Before the PCA, we standardized the variables by subtracting the mean value for each solute and dividing by the standard deviation for each solute. By normalizing the dataset, we removed the weighted influence of different solutes on the basis of their relative concentrations. We then transformed our nine standardized input variables, HCO_3^{-}, F^{-}, Cl^{-}, NO_3^{-}, SO_4^{2-}, Na^{+}, K^{+}, Mg^{2+}, and Ca^{2+}, into nine linear combinations, or principal component (PC) scores. The coefficients, or loadings, for each variable represent the relative importance of each individual variable for computing the PC scores and are used to interpret the meaning of the PCs. The variance summarized by each PC can be expressed as a percentage of the total data variance.

We initially ran a PCA with the complete geochemistry dataset (PC1) and subsequently used those results to identify groundwater (GW)-rich *versus* surface water (SW)-rich sites in the streambed. We then ran a second PCA on the SW-rich sites (PC2) to more clearly identify controls on stream and streambed geochemistry during the storm event. The first PCA focused on spatial variability within the geochemical dataset and the second PCA focused on temporal variability within the geochemical dataset. Further details on site categorization, as well as the results from both PCAs, are described in the Principal Component Analysis: All Sites and Principal Component Analysis: Surface-Water-Rich Sites Sections.

RESULTS

Principal component analysis: all sites

Principal component analysis of all stream and streambed water samples (PC1, $n = 111$) collected during the sampling period showed how solute concentrations in the stream and streambed co-varied in both space and time (Table I and Figure 2). This analysis yielded nine linear combinations (PC); however, only the first two PCs were used in this study. These two PCs accounted for 79% of the variance within the dataset. The first principal component (PC1.1) accounted for 62% of the variance within the complete dataset and is positively correlated

Table I. Loadings and correlation coefficients of solutes for the first two principal components (PC1.1 and PC1.2) for all sites ($n = 111$); all correlation coefficients were significant with p-values < 0.10.

	PC1.1 loadings GW/SW composition		PC1.2 loadings storm dilution function	
Solute	Loadings	Correlation coefficient	Loadings	Correlation coefficient
Ca^{2+}	0.40	0.95	0.20	0.25
Mg^{2+}	0.40	0.95	0.19	0.23
Na^{+}	−0.35	−0.82	0.40	0.50
K^{+}	−0.27	−0.63	0.32	0.40
SO_4^{2-}	0.41	0.96	0.15	0.18
Cl^{-}	−0.34	−0.79	0.44	0.54
F^{-}	0.33	0.79	0.27	0.34
NO_3^{-}	−0.26	−0.62	0.13	0.16
HCO_3^{-}	0.16	0.38	0.60	0.75
Eigenvalue	*5.56*		*1.55*	
% Variance explained	*61.78*		*17.22*	

Italics denote that the rows "eigenvalues" and "percent variance explained" are different variables than the rest of the rows within the column heading for "loadings".

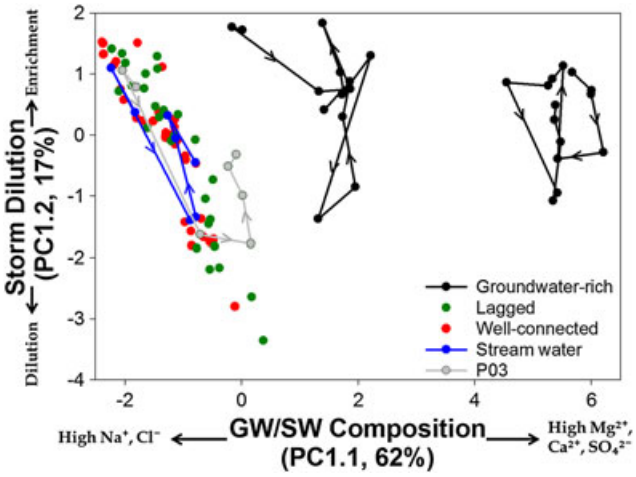

Figure 2. Plot of principal component 2 (PC1.2, storm dilution function) *versus* principal component 1 (PC1.1, GW/SW composition function) from the first principal component analysis (PC1) of all streambed sites and stream water. Blue line represents trajectory of stream water, red and green dots represent SW-rich sites (well-connected and lagged sites, respectively), black lines represent trajectory of GW-rich sites, and grey line represents trajectory of P03, the transitional site. Red and green dots follow trajectory of stream water

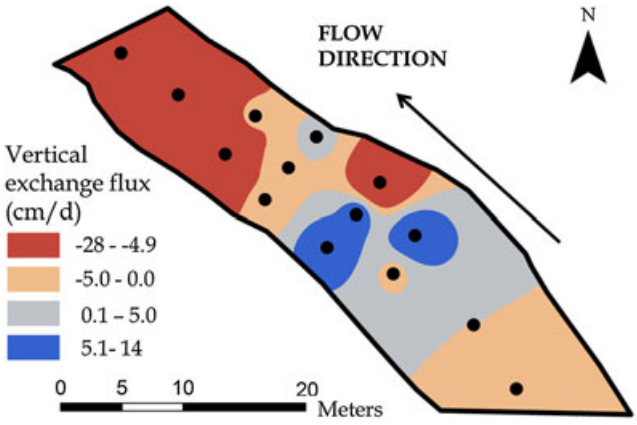

Figure 3. Plot of vertical exchange flux (cm/d) across the streambed averaged between 2.5 and 5.0 cm depths during baseflow conditions Contours were interpolated using ArcGIS. Red indicates upwelling (negative values), and blue indicates downwelling (positive values)

with Ca^{2+}, Mg^{2+}, and SO_4^{2-} and negatively correlated with Na^+ and Cl^- (Table I). PC1.1 is referred to as the 'GW-influence' function, as it represents the spatial influence of relatively $Ca^{2+}/Mg^{2+}/SO_4^{2+}$-poor, Na^+/Cl^--rich surface water and relatively $Ca^{2+}/Mg^{2+}/SO_4^{2-}$-rich, Na^+/Cl^--poor groundwater at each streambed site. This GW-influence function primarily captures spatial differences between sites that have variable contributions of groundwater. Low scores for PC1.1 (<0) indicate sites primarily composed of stream water. Stream water samples had negative PC1.1 scores between −1.8 and −0.8. Streambed sites that stay below or at zero are thus considered SW rich and are designated with green and red points in Figure 2. Positive scores for PC1.1 (>0) indicate hyporheic sites strongly influenced by mixing with groundwater (Figure 2). These sites (P01, P02, P05, and P09) are considered to be GW-rich sites, which are designated with black points in Figure 2. Heat transport modelling results of vertical water exchange show these sites are upwelling, with an average exchange rate of −16 cm/d, during baseflow conditions (Figure 3). P03 is the only transitional site between the SW-rich and GW-rich categories, which is designated with grey points on Figure 2. Although P03 started as an SW-rich site during baseflow conditions, it showed a larger change in PC1.1 scores than the stream and any other SW-rich site during the storm (Figure 2). This large change in GW-influence score suggests that discharge of GW to P03 increased during the storm.

The second principal component (PC1.2) accounted for 17% of the variance within the dataset and is most strongly correlated with concentrations of Na^+, Cl^-, and HCO_3^- (Table I). PC1.2 was primarily used to summarize temporal variations in geochemistry at individual sites during the storm event. The loadings for all solutes for PC1.2 were positive, indicating that all solute concentrations are relatively enriched in samples with high PC1.2 scores (>0) and solute concentrations are relatively dilute when the PC1.2 score is low (<0). PC1.2 is therefore referred to as the 'storm dilution' function, as it represents the dilution of solutes during the storm event and the subsequent re-enrichment as the system rebounds from the storm event.

All streambed pore water and stream water samples initially had storm dilution scores greater than zero, indicating relative enrichment of all ion concentrations before the storm event. The storm dilution score for stream water dropped from 0.4 to −1.6 during the storm, reflecting the dilution of all ions during the event, and rebounded to a value of −0.4 following the event, showing re-enrichment of ions (Figure 2). All streambed pore water showed some degree of overall solute dilution during the storm event that mirrored the stream water response, as indicated by a decrease in the storm dilution score at all sites during the event. However, the GW-rich sites showed a notably smaller dilution response than SW-rich sites (Figure 2), and the majority of GW-rich samples did not dip below zero for PC1.2. Whereas none of the GW-rich sites dipped below the lowest PC1.2 score within the SW samples (−1.6), many SW-rich sites dipped well below that value, with a minimum PC1.2 score of −3.4 for site P12.

Principal component analysis: surface-water-rich sites

The first principal component analysis (PC1) indicates that the majority (62%) of the variance in the complete dataset is associated with the varying spatial influence of GW at the various sites (PC1.1). To tease out temporal relationships associated with the storm event, we removed the GW-rich sites (P01, P02, P05, and P09) as well as transitional site P03 from the dataset for our second PCA (PC2, $n = 77$). By subsetting the dataset in this way, we were able to minimize GW influence and isolate streambed pore water samples that were primarily influenced by stream water infiltration. This allowed us to more closely scrutinize the temporal variability of pore water chemistry at these connected streambed sites during the storm event.

The PC2 analysis yielded two main PCs that accounted for 72% of the variance within the select dataset (Table II and Figure 4). The first PC (PC2.1) accounted for 54% of the variance within the dataset and is similar to PC1.2 in that it is strongly correlated with Na^+, Cl^-, and HCO_3^- and has positive loadings for all solutes (Table II). PC2.1 is therefore referred to as another storm dilution function, as it represents the flushing of streambed sites by dilute event water and the subsequent re-enrichment of solute concentrations as the system rebounds from the storm event. The second PC (PC2.2) accounted for 18% of the variance within the dataset and is most strongly and positively correlated with NO_3^- (Table II). PC2.2 is therefore referred to as the 'nitrate' function, as it represents the combined influences of initial enrichment, subsequent dilution, and biogeochemical processing of NO_3^- before and after the storm event (Figure 4).

On the basis of PC2, we were able to categorize the SW-rich streambed sites into two groups: 'well-connected sites' and 'lagged sites'. Although the majority of the variance in the select dataset can be found in the storm dilution component (PC2.1), the nitrate component (PC2.2) was primarily used to differentiate between well-connected and lagged sites (Figure 4). Well-connected sites showed mostly positive nitrate scores both pre-event and post-event that varied from −0.15 to 2.1. These sites were generally located at the head of the riffle bedform, at sites P04, P06, P07, P08, and P10, where heat transport modelling shows SW was downwelling during baseflow with an average exchange rate of 8.0 cm/d (Figure 3). In contrast, lagged sites had a positive nitrate score during baseflow conditions but became and stayed negative throughout the storm event (Figure 4). These sites were generally located at the tail of the riffle bedform, at sites P11, P12, P13, and P14, where heat transport modelling shows streambed water was upwelling during baseflow with an average exchange rate of −13 cm/d (Figure 3).

Streambed chemistry in lagged and well-connected sites

To summarize differences in the biogeochemical response of well-connected *versus* lagged sites throughout the storm, we conducted two tailed *t*-tests on biogeochemically reactive solutes, K^+, NO_3^-, and SO_4^{2-}, as well as pH and DO, between the two categories (Table III). We used a *p*-value of 0.10 as a significance threshold because of the low number of sample points. At baseflow conditions, the biogeochemically reactive solutes (except SO_4^{2-}), pH, and DO were significantly different between well-connected and lagged sites ($p < 0.10$). During the rising limb of the storm, there were no significant biogeochemical differences between the well-connected and lagged sites. During the first sample period during the receding limb of the hydrograph, all biogeochemically reactive parameters became significantly different, except K^+. During the second, third, and fourth sample periods of the receding limb, almost all biogeochemically reactive parameters were significantly different between the well-connected and lagged sites ($p < 0.10$). By the last sampling period, the differences in solute concentrations between the well-connected and lagged sites returned to pre-event conditions (Table III).

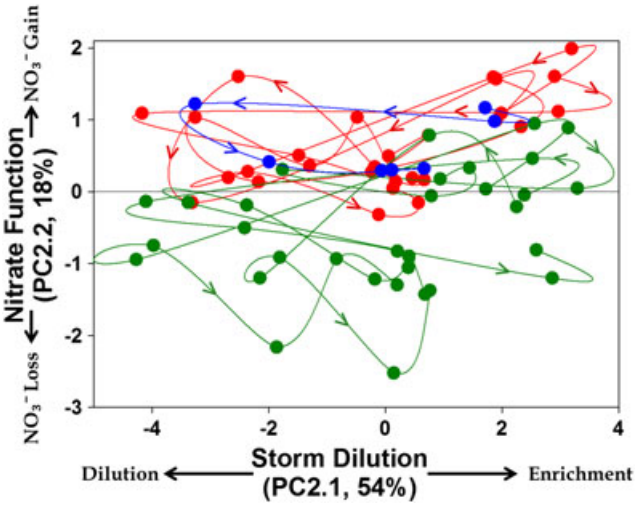

Figure 4. Plot of principal component 2 (PC2.2, nitrate function) *versus* principal component 1 (PC2.1, storm dilution function) from the second principal component analysis (PC2) of SW-rich sites and stream water. Blue line represents stream water, red line represents well-connected sites, and green represents lagged sites. All lines start in the upper right corner, and arrows indicate overall trajectories

Table II. Loadings and correlation coefficients of solutes for the first two principal components for surface-water-rich sites (PC2.1 and PC2.2, $n = 77$).

	PC2.1 loadings storm dilution function		PC2.1 loadings nitrate function	
Solute	Loadings	Correlation coefficient	Loadings	Correlation coefficient
Ca^{2+}	0.36	0.79	−0.38	-0.49
Mg^{2+}	0.34	0.75	−0.05	*ns
Na^+	0.43	0.95	0.19	*ns
K^+	0.20	0.45	−0.39	−0.51
$SO4^{2-}$	0.41	0.89	0.16	*ns
Cl^-	0.43	0.96	0.16	*ns
F^-	0.25	0.55	0.34	0.44
$NO3^-$	0.16	0.34	0.50	0.65
$HCO3^-$	0.30	0.66	−0.49	−0.62
Eigenvalue	*4.89*		*1.65*	
% Variance explained	*54.28*		*18.28*	

*ns, not significant correlation coefficients with *p*-values > 0.10.

Table III. Comparison of mean concentrations for biogeochemically reactive solutes at well-connected (P04, P06, P07, P08, and P10) *versus* lagged (P11, P12, P13, and P14) streambed sites

Sampling period	1	2	3	4	5	6	7
	Baseflow	Rising limb of storm	Receding limb of storm				
SO_4^{2-}	*ns	*ns	47.27, 40.48 (0.10)	53.28, 47.59 (0.04)	58.78, 52.67 (0.04)	61.17, 56.74 (0.07)	*ns
K^+	2.03, 2.23 (0.01)	*ns	*ns	1.56, 1.83 (0.09)	1.86, 2.5 (0.07)	1.69, 2.08 (0.01)	1.84, 2.38 (0.01)
NO_3^-	2.31, 0.95 (0.07)	*ns	1.68, 0.62 (0.02)	1.74, 0.59 (0.00)	2.20, 0.71 (0.00)	2.51, 0.84 (0.00)	1.99, 0.72 (0.02)
pH	7.87, 7.62 (0.07)	*ns	8.00, 7.81 (0.06)	7.95, 7.62 (0.03)	8.05, 7.62 (0.03)	*ns	8.00, 7.68 (0.10)
DO	5.02, 2.19 (0.03)	*ns	5.16, 2.31 (0.05)	6.81, 2.01 (0.02)	7.11, 2.13 (0.00)	6.34, 2.19 (0.01)	6.221, 2.53 (0.03)

Average concentrations are reported for the well-connected and lagged sites, respectively, if mean differences were significant ($p < 0.10$); p-values are reported in parentheses.
*ns, no significant difference in concentration between groups.

Baseflow stream and streambed geochemistry

Solute concentrations in stream and streambed pore water reflect the patterns summarized using the PCA. All solute concentrations in SW samples taken at both the head and tail of the 30 m study reach were within 5% during each sampling period, indicating the stream water chemistry was spatially uniform across the study reach. During the baseflow survey, SW chemistry was dominated by SO_4^{2-} (74.7 mg/l) and Ca^{2+} (77.5 mg/l) and had an SC value of 540 μS/cm, DO concentration of 12.1 mg/l, NO_3^- concentration of 2.2 mg/l, and Cl^- concentration of 30.1 mg/l.

In the baseflow survey, we saw relatively uniform, SW-rich pore water geochemistry across the riffle bedform at a screened depth centred at 15 cm below the sediment–water interface, with the exception of zones of GW discharge that were spatially oriented towards the head of the riffle and on the outside of the meander (sites P01, P02, P05, and P09; Figure 5). These sites are recognized as GW-rich sites in PC1.1. The zones of GW discharge had relatively high concentrations of SO_4^{2-}, Ca^{2+}, and Mg^{2+} (Figure 5A for SO_4^{2-}) and low concentrations of Na^+ and Cl^-, relative to other streambed sites (Figure 5B for Cl^-). The GW-rich sites had high SC values ranging from 805 to 1945 μS/cm, whereas the rest of the streambed sites had stream-like SC values from 580 to 629 μS/cm. Concentrations of DO ranged from 0.8 to 4.6 mg/l in the GW-rich sites and ranged from 1.5 to 9.1 mg/l in the rest of the streambed sites (Figure 5D).

Streambed pore water geochemistry outside of zones affected by GW discharge showed some spatial organization around the riffle bedform at baseflow conditions. This spatial organization was represented with well-connected and lagged sites in PC2.2. At baseflow, mean concentrations of biogeochemically reactive ions NO_3^- and K^+ as well as pH and DO were significantly different ($p < 0.10$) in SW-rich sites above the riffle relative to SW-rich sites below the riffle, with higher NO_3^- at the upstream sites and higher K^+ at the downstream sites (Table III; Figure 5C for NO_3^- and Figure 5D for DO).

Storm event stream and streambed geochemistry

Stream water showed an initial increase in SC and concentrations of K^+, HCO_3^-, Na^+ (~10% increase), and NO_3^- (50% increase) during the rising limb of the storm but a decrease in all solute concentrations (between 7% and 54%) during the first sampling of the storm recession (Figures 6 and 7 for Cl^-, SO_4^{2-}, and NO_3^-). As the stream stage receded over the subsequent three sampling dates, the solute concentrations in the stream increased steadily (Figures 6 and 7). None of the solute concentrations in the stream water completely returned to pre-event baseflow concentrations (except Mg^{2+}) during the sampling period.

Groundwater-rich sites (P01, P02, P05, and P09) showed minimal geochemical response during the storm event, relative to the SW-rich sites (Figures 2 and 6). These sites had the highest concentrations of Mg^{2+}, Ca^{2+}, and SO_4^{2-} in the streambed, which on average increased from baseflow sampling to the final post-event sampling period.

Outside the streambed zone showing influence of GW discharge, the geochemistry at streambed sites reflected the influence of stream water concentration at varying time scales as well as bedform morphology. Sites upstream of the riffle bedform (well-connected sites) generally responded faster to changes in stream water solute concentrations, whereas downstream sites (lagged sites) showed a delay in response. For instance, concentrations of Cl^-, a conservative solute, were similar between well-connected and lagged sites during baseflow conditions but became significantly different during the storm (Table III; Figure 6). As Figures 6 and 7 demonstrate, well-connected sites followed changes in stream water closely during the receding limb, whereas lagged sites presented the solute concentrations of SW and well-connected sites from previous sampling periods. Similarly, although the storm onset caused initial uniformity across well-connected and lagged sites, the storm recession yielded spatial differences in non-conservative ion concentrations. For instance, NO_3^-, SO_4^{2-}, and DO concentrations as well as pH were consistently higher in well-connected sites, whereas

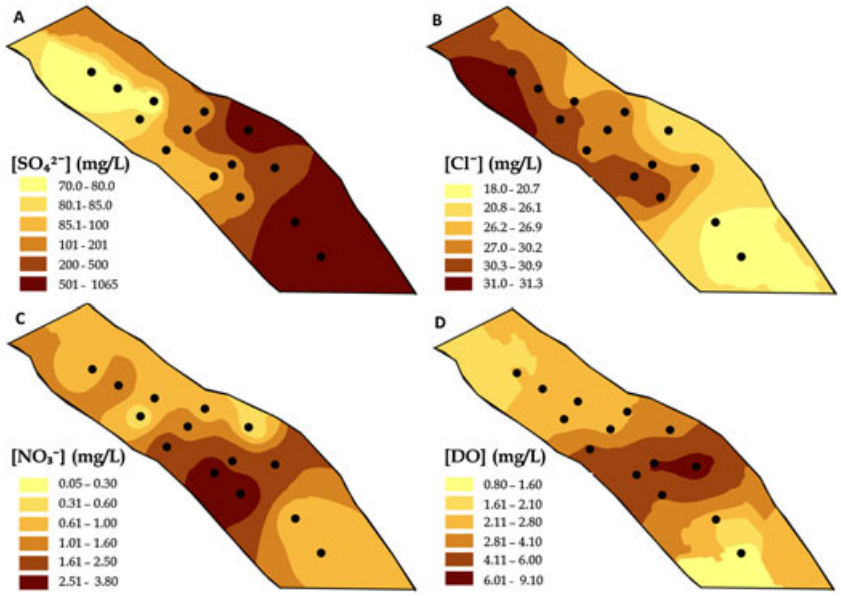

Figure 5. Streambed concentrations of (A) sulfate, (B) chloride, (C) nitrate, and (D) dissolved oxygen, during baseflow conditions. Lighter colours represent lower concentrations and darker colours represent higher concentrations. Contours were interpolated using ArcGIS

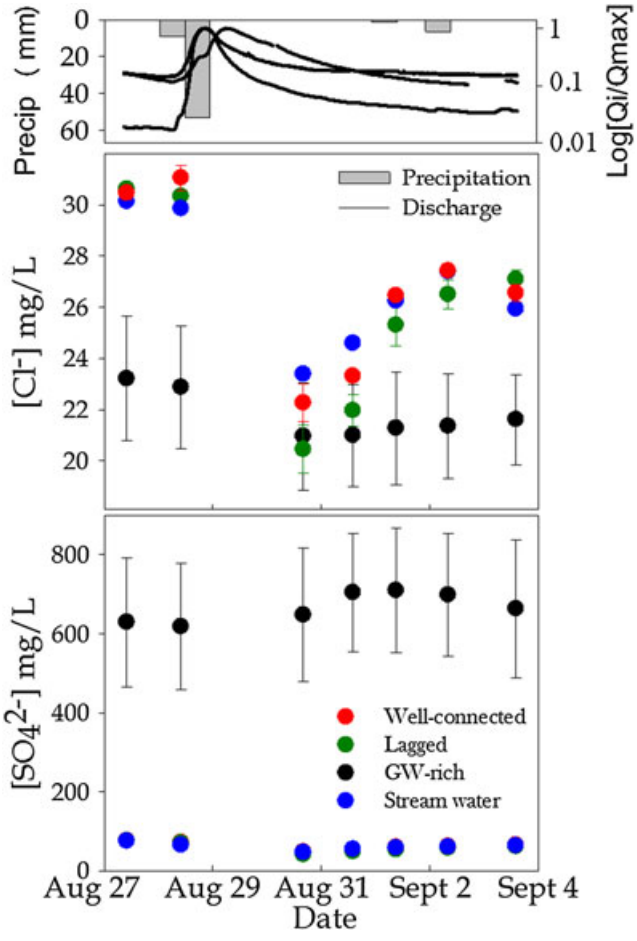

Figure 6. (Top) Daily precipitation inputs from nearby National Oceanic and Atmospheric Administration meteorological station. Three normalized stream hydrographs from nearby United States Geological Survey stream gauge stations. (Middle) Time-series plot of mean chloride concentrations for GW-rich sites (black), lagged sites (green), well-connected sites (red), and stream water (blue). Error bars represent standard error. (Bottom) Time-series plot of mean sulfate concentrations, with same colour designations as middle plot

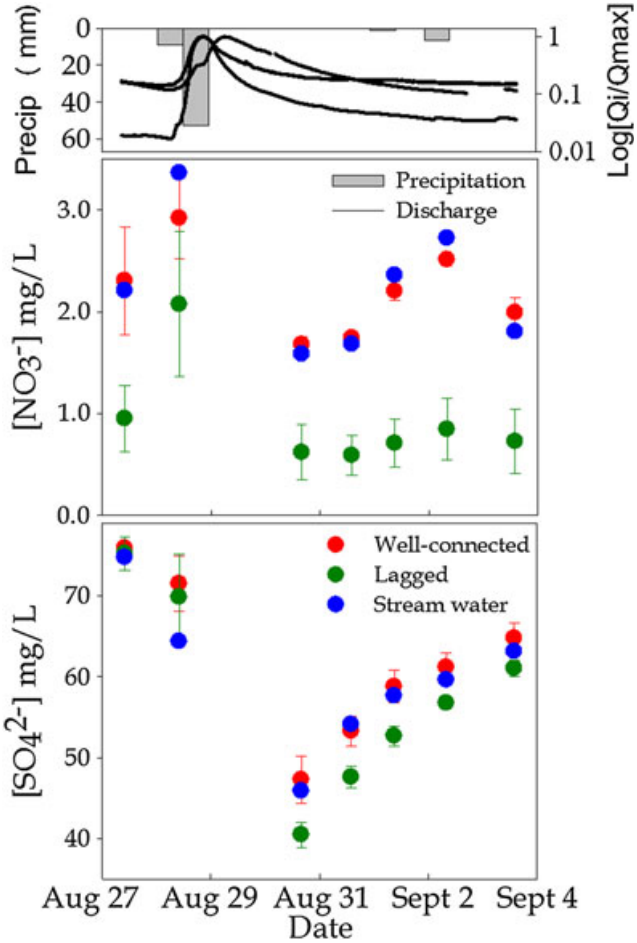

Figure 7. (Top) Daily precipitation inputs from nearby National Oceanic and Atmospheric Administration meteorological station. Three normalized stream hydrographs from nearby United States Geological Survey stream gauge stations. (Middle) Time series plot of mean nitrate concentrations for lagged sites (green), well-connected sites (red), and stream water (blue). Error bars represent standard error. (Bottom) Time series plot of mean sulfate concentrations, with same colour designations as middle plot

K^+ concentrations were consistently higher in lagged sites throughout the receding limb of the storm event (Table III; Figure 7 for NO_3^-).

Chemical variability versus depth of sampling

We installed nested piezometers at select GW-rich, well-connected, and lagged sites (P02, P05, P07, and P11) to test chemical variability with depth (from 15 to 30 cm). The temporal variability, or range in concentrations of SO_4^{2-}, a GW indicator, was highest at the 15-cm depth at the GW-rich nested sites (P02 and P05) but lowest at the lagged (P11) and well-connected sites (P07; Figure 8). Concentrations of SO_4^{2-} increased with depth at GW-rich sites but stayed consistent with depth for well-connected and lagged sites (Figure 8). The temporal variability, or range in concentrations of NO_3^-, an SW indicator, was greatest at 15 cm for all nested piezometers, except P07 at the well-connected site (P07). With greater depth, the range decreased, except at the well-connected site. Concentrations of NO_3^- decreased with depth at all nested sites, except the well-connected site (Figure 8).

DISCUSSION

Source delineation

At baseflow conditions, streambed sites can be divided into SW-rich *versus* GW-rich sites on the basis of geochemistry (Figure 5). SW-rich sites have higher Na^+, Cl^-, NO_3^-, and DO concentrations, whereas GW-rich sites have higher SC values and Ca^{2+}, Mg^{2+}, and SO_4^{2-} concentrations. This geochemical distinction between SW-rich and GW-rich sites was confirmed by PC1.1 (Figure 2). Within the group of SW-rich sites, NO_3^- and DO concentrations and pH values are generally higher in streambed sites upstream of the riffle bedform (well-connected sites) and lower in sites downstream of the riffle bedform (lagged sites; Figure 5; column 1 of Table III). Studies have shown similar spatial patterns along riffle–pool bedform morphology during baseflow conditions (e.g. Kasahara and Hill, 2006; Lautz and Fanelli, 2008). Water infiltrates into the streambed upstream of the riffle, moves along a subsurface flowpath, and upwells back into the stream downstream of the riffle, with depletion of DO and NO_3^- concentrations and decrease in pH along the flowpath in response to microbial use of solutes as electron acceptors during the oxidation of organic carbon, and thus acidification, in the streambed. Our calculated vertical exchange rates at baseflow support these patterns as well (Figure 3).

The presence of spatially distributed points of anomalous GW inputs (P01, P02, P05, and P09), as opposed to uniform and spatially diffused GW inputs, has been seen in other studies (e.g. Conant, 2004; Conant *et al.*, 2007; Lautz and Ribaudo, 2012). These anomalous GW inputs may be a result of the local-scale geology, such as zones of high hydraulic conductivity, which allow for high rates of groundwater discharge. This distribution of chemistry from SW and GW contributions at baseflow conditions suggests there are two main physical drivers in hyporheic geochemistry: (1) the bedform morphology, which drives local subsurface flowpaths, around a pool–riffle–pool bedform in our study, and (2) anomalous groundwater discharge points that provide a GW chemical signature to the hyporheic zone, which are located upstream of the riffle and to the outer edge of the meander in our study.

Event response

On the basis of our temporal geochemical analysis, it is apparent the dominant driver of hyporheic exchange during the storm event is an increase in stream stage. At the storm onset, a rise in stream stage causes the streambed to be inundated with dilute event water at all SW-rich sites (Figures 6 and 7; column 2 of Table III). This is seen in PC1.2 and PC2.1 (storm dilution functions), as the streambed sites (well-connected and lagged sites) show dilute pore water chemistry that reflects stream water dilution during the event (Figures 2, 4, 6, and 7). Further, biogeochemically reactive solutes K^+ and NO_3^- as well as pH and DO were significantly different between well-connected and lagged sites before the storm but became more uniform across these sites during the rising limb (Table III). This suggests either the flowpaths have decreased in residence time from an increase in stream

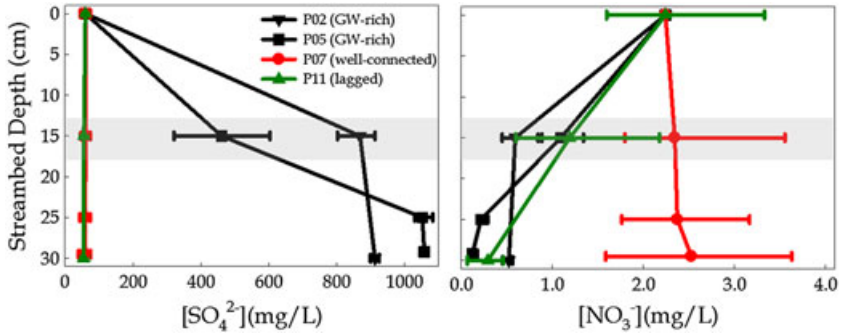

Figure 8. Plots of mean sulfate (left) and nitrate (right) concentrations for select GW-rich (black), well-connected (red), and lagged (green) sites at streambed depths centred at 15, 25, and 30 cm (5 cm screened piezometers). Error bars represent minimum and maximum values for each category. Grey box centred around 15 cm depth represents standard depth of pore water sampling. Depth of zero represents stream water

stage or the streambed has been uniformly inundated by stream water. Analogous hyporheic response to rapidly changing stream stage has been shown in other hyporheic exchange studies; for example, Arntzen *et al.* (2006), Sawyer *et al.* (2009), and Francis *et al.* (2010) all showed through vertical exchange measurements that increases in stream stage, from daily dam regulated flow release, push stream water into the streambed, even in naturally GW gaining systems (Sawyer *et al.*, 2009). Malcolm *et al.* (2004, 2006) also saw an increase in SW contributions in the streambed during periods of higher stream flow during storm events. In this study, GW-rich sites do not show as much chemical change from infiltrating stream water (Figures 2 and 6), which may be because the large proportion of GW in the streambed pore water at these locations masks the SW signal. The minimal geochemical response at the GW-rich sites we report could also be a product of a sampling period that was too short to detect the full effects of storm water inputs to the aquifer and thus any longer term changes in groundwater chemistry related to the storm event.

Spatial differences in the response of hyporheic exchange during the storm event can be summarized by dividing the SW-rich sites into two groups we called well-connected and lagged sites, which are differentiated by the patterns seen in PC2.2 (nitrate function; Figure 4). Throughout the event, well-connected sites show a similar composition to stream chemistry, suggesting rapid hyporheic exchange during the storm (Figures 6 and 7). Lagged sites generally show similar dilution/enrichment patterns to well-connected sites but show lower and/or lagged solute concentrations relative to the stream and well-connected sites throughout the event (Figures 6 and 7; Table III). The distribution of well-connected and lagged sites is tied to the bedform morphology, as well-connected sites fall within and above the riffle, whereas lagged sites fall below the riffle bedform. The lagged response in the downstream sites is thus most likely due to the longer subsurface flowpath for these sites, which causes a lagged arrival of dilute event water and enriching post-event water. Thus, whereas the stream and well-connected sites are concurrently recovering from event dilution and re-enrichment as the storm passes, the lagged sites reflect the stream chemistry in the recent past (e.g. the prior day). We therefore see concentration differences in conservative solutes such as Cl^- between well-connected and lagged sites during event dilution and recovery (Figure 6).

Concentrations in biogeochemically reactive solutes, K^+ and NO_3^-, stay significantly different between well-connected and lagged sites throughout the entire sampling period, except during initial flushing of the streambed at the storm onset (Table III). We hypothesize this is due to the stream stage rising rapidly during storm onset, pushing stream water into the streambed, temporarily making the streambed chemically uniform at these SW-rich sites. As the stream stage recedes, however, the localized subsurface flowpaths across the riffle dominate the movement of hyporheic zone water, reproducing differences in biogeochemically reactive solutes between the two groups.

The differences in concentrations of biogeochemically reactive K^+ and DO between well-connected and lagged sites become greater from baseflow to the final post-event sampling (Table III). Although the differences in NO_3^- concentrations between well-connected and lagged sites did not become greater from baseflow to final post-event sampling, concentrations were relatively low at the lagged sites throughout the receding limb of the storm hydrograph, whereas connected sites began to recover in NO_3^- concentrations (Figure 7; Table III). We hypothesize the spatial difference in these biogeochemically reactive solutes is due to changes in microbial processing along the subsurface flowpaths. Although we did not measure dissolved organic carbon (DOC), we hypothesize a rapid influx of DOC in the stream during the storm may have occurred, as seen in several studies (Hinton *et al.*, 1997; Inamdar *et al.*, 2004). The hyporheic zone may have also received an increased influx of DOC, which is a main component needed for microbial processing. The effects of increased DOC concentrations may be more apparent at the downstream end of the hyporheic flowpaths, where longer hyporheic residence time may allow for greater net effect of microbial processes on pore water geochemistry. Increased microbial processing requires oxygen or other electron acceptors and thus may produce environments suitable for denitrification and acidification. The positive relationship between residence time and microbial processing has been shown in other studies (e.g. Zarnetske *et al.*, 2011; Briggs *et al.*, 2012). Zarnetske *et al.* (2011) showed that the greatest net decline in NO_3^- concentrations in the hyporheic zone occurred at the longest residence times within subsurface flowpaths along a stream and adjacent gravel bar.

During most of the sampling regime, DO concentrations increased in the well-connected sites but stayed fairly constant, and much lower, in the lagged sites (Table III). Concentrations in DO may increase in the upstream subsurface section because of the constant and perhaps enhanced downwelling of more turbulent, and thus DO-rich, stream water. Most likely, this steady and increased source of DO at the upstream end provides enough oxygen for respiration to occur so that alternate electron acceptors are not utilized until farther along in the subsurface flowpath.

Sulfate concentrations start uniform between lagged and well-connected sites at baseflow (Table III), most likely because the presence of SO_4^{2-}-rich gypsum weathering contributes high amounts of SO_4^{2-} to the stream system. However, during the receding limb of the storm hydrograph, the difference in SO_4^{2-} concentrations between lagged and well-connected sites becomes significant (Table III). This is most likely due to SO_4^{2-} reduction, as we see lower concentrations of SO_4^{2-} in the downstream sites. By the end of the sampling regime, as the stage recedes, SO_4^{2-} concentrations have returned to pre-event conditions (Table III), again displaying the dominance of bedrock weathering across the study reach.

As there is more cumulative microbial processing at the downstream sites due to flowpath length, the dominant

process of NO_3^- and SO_4^{2-} reduction is reflected in higher K^+ concentrations (Table III). Concentrations of reactive K^+ are larger in the downstream sites at baseflow, and the difference becomes greater throughout the storm. We hypothesize that as DOC concentrations increase, mineralization of organic matter increases as microbial processing increases. This mineralization of organic matter releases K^+ found in the organic matter (Blair, 1988), and the net effect of the longer subsurface flowpath at the downstream sites allows for higher concentrations of K^+.

There is a range in streambed storm responses within streambed groups (well-connected, lagged, and GW-rich groups), suggesting a gradation of the stream–streambed connectivity and GW influence. Our results further show that this gradation of geochemical drivers in the streambed shifts throughout the storm event. For example, we observed signs of the expansion of groundwater influence across the streambed, most notably at the head of the riffle at P03. Site P03 showed chemistry similar to SW-rich sites at pre-event baseflow conditions (PC1.1 = −1.8, low concentrations of Mg^{2+}, Ca^{2+}, HCO_3^-, and SO_4^{2-} and high concentrations of Na^+ and Cl^-; Figure 2). However, during the storm, the solute concentrations at P03 became increasingly more similar to other GW-rich sites (PC1.1 > 0, high concentrations of Mg^{2+}, Ca^{2+}, HCO_3^-, and SO_4^{2-} and low concentrations of Na^+ and Cl^-). This shift in pore water chemistry suggests the zone of GW influence increased during the storm event, as P03 is adjacent to or at the edge of consistently GW-rich regions (P01, P02, P05, and P09). Several modelling studies have also reported an increase in the area of GW discharge during periods of changing stream stage (e.g. Wondzell and Swanson, 1996; Wroblicky *et al.*, 1998; Shibata *et al.*, 2004). Cardenas and Wilson (2007) and Boano *et al.* (2008) showed that a rise in the water table in the riparian zone or nearby hillslope increases the hydraulic gradient towards the stream, thus driving GW flowpaths towards the streambed and compressing the hyporheic zone. We hypothesize this rapid increase in hydraulic gradient towards the stream is causing the increase of GW influence at P03 (Figure 9).

Groundwater-rich sites do not show a large chemical response from downwelling SW (Figures 2 and 6), and thus, we believe the GW source overwhelms the stream signal at those particular sites during the storm. We hypothesize that SW represents a sufficiently small portion of the bed chemistry at the GW-rich sites so that temporal chemistry changes in any downwelling SW do not have a large influence on the pore water chemistry. Although the increase in stream stage during the storm may reverse hydraulic gradients in some regions of the bed, or increase gradients at initially downwelling sites, we hypothesize that the rising stream stage is not sufficient to reverse the hydraulic gradient at the focused groundwater discharge zones. As a result, GW-rich sites maintain an upward gradient throughout the storm event and thus show no geochemical signs of an influx of large proportions of SW. The cause of the focused GW upwelling may be local-scale geology, such as localized areas of higher hydraulic conductivity.

Conceptual model

The coupling of bedform morphology-driven hyporheic exchange with localized GW discharge at our study site creates complex geochemical responses to fluctuating stream stage in the streambed. In this section, we present a summary, or conceptual model, of hyporheic exchange patterns occurring in the streambed during baseflow, storm onset, and storm recession, and the associated geochemical response within well-connected, lagged, and GW-rich sites.

At baseflow, GW-rich sites are localized towards the upstream end of the streambed (Figure 9A), most likely due to local-scale geology, such as zones of high hydraulic conductivity. SW-rich sites, on the other hand, show spatial geochemical patterns driven by the riffle bedform (Figure 5). Hyporheic flowpaths connect the sites at the upstream end of the riffle to the sites at the downstream end of the riffle, and we see expected patterns in biogeochemically reactive solutes (Kasahara and Hill, 2006; Lautz and Fanelli, 2008).

During the storm, differences in pore water geochemistry measured between upstream and downstream SW-rich sites (Figures 6 and 7; Table III) are from (1) differences in source water along the hyporheic flowpaths due to a changing SW chemistry during the storm and (2) biogeochemical processes occurring along subsurface flowpaths within the streambed, such as microbial respiration and the associated consumption of DO, NO_3^- and SO_4^{2-} reduction, production of inorganic carbon, and decline in pH.

At storm onset, stream stage rises, increasing the hydraulic head at the streambed interface, causing rapid

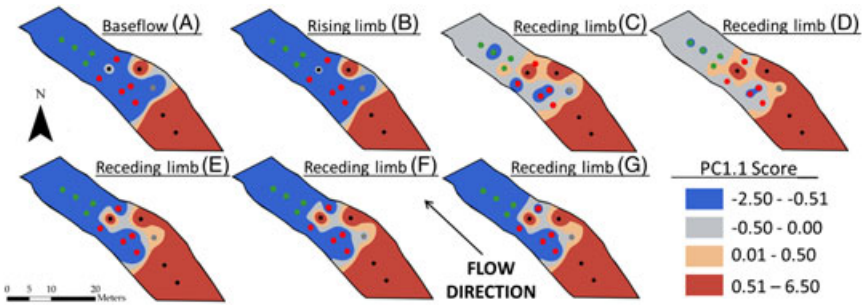

Figure 9. Streambed maps of the first principal component score (PC1.1 GW/SW composition score) for the first principal component analysis (PC1) over each sample date (A–G). Each piezometer site is labelled as either GW-rich (black), lagged (green), or well-connected (red). Blue contours represent more surface water influence, and red contours represent more groundwater influence. Contours were interpolated using ArcGIS

influx of event water into the hyporheic zone. There are two possible explanations for such inundation of stream water during the rising limb. First, at streambed locations with downwelling or weak upwelling exchange rates during baseflow (Figure 3), we hypothesize that hydraulic gradients are increased or reversed, respectively, and these regions of the streambed are rapidly inundated with dilute event water. Alternatively, rising stage increases flow rates along shallow hyporheic flowpaths such that residences times are short and biogeochemical processes leave a minimal imprint on hyporheic water chemistry. As a result, SW-rich sites initially show similar chemical responses during storm onset, for example, a decrease in SO_4^{2-} concentrations and increase in NO_3^- concentrations (Figure 7). The influence of biochemical processes occurring along the hyporheic flowpaths is diminished at this time because of rapid inundation of stream water. This briefly produces almost uniform geochemistry across the SW-rich hyporheic zone (Table III). The GW-rich sites, however, still reflect only minor influence of stream water. At these locations, we hypothesize upwelling is maintained despite the increase in stage and the GW geochemical signal remains strong (Figure 9B).

During storm recession, the hydraulic head at the streambed interface decreases as the stream stage decreases and the subsurface flowpaths driven by the riffle bedform once again become the main driver of hyporheic zone chemistry at the SW-rich sites. During this time, hyporheic flowpaths receive stream water that has a fluctuating geochemical composition due to a fluctuating composition of precipitation, hillslope runoff, and baseflow groundwater as the system responds to the recent storm event. Because stream water chemistry varies temporally during storm recession, stream water that downwells into the streambed at one time is not chemically the same as the stream water that downwells at a time step later. Therefore, at one point, the chemistry of the pore water at the upstream end of the riffle more closely reflects current SW chemistry, whereas the chemistry of the pore water at the downstream end of the riffle reflects the chemistry of surface water that entered the streambed at an earlier time step (Figures 6 and 7).

The subsurface flowpaths driven by the riffle bedform are the main drivers of hyporheic exchange at the SW-rich sites during the storm recession, and the residence time of hyporheic flowpaths produces differences in concentrations of biogeochemically reactive solutes between upstream and downstream sites (Table III). By the end of the study period, towards the end of storm recession, the SW chemistry began to stabilize and non-conservative solute concentrations, such as Cl^-, became uniform across the upstream and downstream streambed sites (Figure 6). However, the mean value of biogeochemically reactive solutes K^+ and DO was more different between upstream and downstream sites after the storm event, relative to before (Table III). Further, NO_3^- concentrations were more significantly different (smaller p-value) between upstream and downstream sites after the storm, relative to before (Table III). This suggests the disturbance from the storm event had left the downstream system at a new biological condition, perhaps from an influx of DOC. Alternatively, the site had not fully recovered by the end of sampling.

CONCLUSIONS

This study examined the temporal and spatial responses of hyporheic zone geochemistry during a storm event. The objectives of this study were to (1) characterize spatial vertical water exchange rates and geochemical patterns in the hyporheic zone around a pool–riffle–pool bedform during baseflow and (2) use results from PCA and time-series geochemical analyses to conceptualize how different regions of the hyporheic zone respond to storm events. The primary drivers of spatial and temporal variability in streambed geochemistry around a riffle during baseflow conditions and storm events are bedform morphology, chemical composition of GW discharge and varying composition of stream water from storm inputs.

Stream water enters the streambed at the head of the riffle, as a result of the increase in slope across the bedform, and upwells back into the stream at the tail of the riffle. Streambed sites upstream of the riffle bedform reflected conservative solute concentrations in the stream throughout storm events, whereas sites downstream of the riffle showed a lagged response to changes in solute concentrations in the stream water. We hypothesize that this is most likely due to the subsurface residence time along flowpaths connecting locations where stream water enters the streambed above the riffle to locations where that water discharges back to the stream at the tail of the riffle. Temporal variations in non-conservative solutes, however, suggest different influences of streambed processes are taking place spatially during the storm event. Whereas upstream sites mirror non-conservative stream solute concentrations throughout the storm, downstream sites reflect the influence of oxygen consumption, acidification, sulfate reduction, and denitrification in the hyporheic zone, which may be enhanced because of an increase in DOC from the storm event and from a longer residence time of pore water.

The other driver of spatial variability in the streambed is from the influence of groundwater discharge. Although the increase in stream stage may drive surface water into the streambed at the groundwater discharge points, the water table in the riparian zone or nearby hillslope likely rises in response to the storm event, increasing the hydraulic gradient towards the stream, driving GW flowpaths towards the streambed, compressing the hyporheic zone and diminishing the geochemical signature of surface water in the streambed at these locations. Because the hydraulic gradient towards the stream presumably increases throughout the storm, the zone of groundwater influence within the streambed expands, elevating Ca^{2+} and SO_4^{2-} concentrations in neighbouring sites.

From this study, it is apparent that the aforementioned geochemical drivers persist throughout rapid fluctuations in the stream stage, although the relative influence of these drivers shifts at some locations over time. For instance,

biogeochemical differences along subsurface hyporheic flowpaths appear and disappear on much shorter time scales than GW influence to sites neighbouring GW discharge points during storms.

Few hyporheic zone studies to date have focused on temporal geochemical dynamics during storm events, most likely as a result of the relatively recent interest in hyporheic zone research and the difficulty of storm sampling. This type of study provides an opportunity for researchers to better understand the hyporheic zone response during periods where watershed-scale solute export is at a maximum. Although sampling was limited by accessibility to the mini-piezometers during Tropical Storm Irene, this study showed that spatial geochemical and nutrient processing patterns in the hyporheic zone stay persistent during periods of fluctuating stream stage, which suggests that the hyporheic zone is an important area for biogeochemical processing in the stream ecosystem across non-steady-state flow conditions.

ACKNOWLEDGEMENTS

This material is based upon work supported by the National Science Foundation under Grant No. EAR-0911612 and the Syracuse Center of Excellence, through the Collaborative Activities for Research and Technology Innovation (CARTI) program. We would like to thank Martin Briggs, AnneMarie Glose, Ryan Gordon, and Sarah Ledford for work in the field as well as two anonymous reviewers who provided valuable comments on the manuscript.

REFERENCES

Arntzen E, Geist DR, Dresel PR. 2006. Effects of fluctuating river flow on groundwater-surface water mixing in the hyporheic zone of a regulated, large cobble bed river. *River Research and Applications* **22**: 937–946.

Blair JM. 1988. Nutrient release from decomposing foliar litter of three tree species with special reference to calcium, magnesium and potassium dynamics. *Plant and Soil* **110**: 49–55.

Boano F, Revelli R, Ridolfi L. 2007. Bedform-induced hyporheic exchange with unsteady flows. *Advances in Water Resources* **30**: 148–156.

Boano F, Revelli R, Ridolfi L. 2008. Reduction of the hyporheic zone volume due to the stream-aquifer interaction. *Geophysical Research Letters* **35**: L09401.

Boano F, Revelli R, Ridolfi L. 2010. Effect of streamflow stochasticity on bedform-driven hyporheic exchange. *Advances in Water Resources* **33**: 1367–1374.

Boulton AJ. 2007. Hyporheic rehabilitation in rivers: restoring vertical connectivity. *Freshwater Biology* **52**: 632–650 DOI: 10.1111/j.1365-2427.2006.01710.x

Boulton AJ, Findlay S, Marmonier P, Stanley EH, Valett HM. 1998. The functional significance of the hyporheic zone in streams and rivers. *Annual Review of Ecology, Evolution, and Systematics* **29**: 59–81.

Briggs MA, Lautz LK, McKenzie JM, Gordon RP, Hare D. 2012. Using high-resolution distributed temperature sensing to quantify spatial and temporal variability in vertical hyporheic flux. *Water Resources Research* **48**: W02527, DOI: 10.1029/2011WR011227

Cardenas MB, Wilson JL. 2007. Exchange across a sediment–water interface with ambient groundwater discharge. *Journal of Hydrology* **346**: 69–80. http://dx.doi.org/10.1016/j.jhydrol.2007.08.019

Conant BJ. 2004. Delineating and quantifying ground water discharge zones using streambed temperatures. *Ground Water* **42**: 243–257.

Conant BJ, Cherry A, Gillham RW. 2007. A PCE groundwater plume discharging to a river: Influence of the streambed and near-river zone on contaminant distributions. *Contaminant Hydrology* **73**: 249–279.

Creed IF, Band LE. 1998. Export of nitrogen from catchments within a temperate forest: evidence for a unifying mechanism regulated by variable source area dynamics. *Water Resources Research* **34**: 3105–3120. DOI: 10.1029/98WR0192.

D'Angelo DJ, Webster JR, Gregory SV, Meyer JL. 1993. Transient storage in Appalachian and Cascade mountain streams as related to hydraulic characteristics. *Journal of the North American Benthological Society* **3**: 223–235.

Fanelli RM, Lautz LK. 2008. Patterns of water, heat, and solute flux through streambeds around small dams. *Ground Water* **46**: 671–687.

Francis BA, Francis LK, Cardenas MB. 2010. Water table dynamics and groundwater–surface water interaction during filling and draining of a large fluvial island due to dam-induced river stage fluctuations. *Water Resources Research* **46**: W07513. DOI: 10.1029/2009WR008694.

Fritz BG, Arntzen EV. 2007. Effect of rapidly changing river stage on uranium flux through the hyporheic zone. *Ground Water* **45**: 753–760.

Gerecht KE, Cardenas MB, Guswa AJ, Sawyer AH, Nowinski JD, Swanson TE. 2011. Dynamics of hyporheic flow and heat transport across a bed-to-bank continuum in a large regulated river. *Water Resources Research* **47**: W03524. DOI: 10.1029/2010WR009794.

Gooseff MN. 2010. Defining hyporheic zones – advancing our conceptual and operational definitions of where stream water and groundwater meet. *Geography Compass* **4**: 945–955.

Gordon RP, Lautz LK, Briggs MA, McKenzie JM. 2012. Automated calculation of vertical pore-water flux from field temperature time series using the VFLUX method and computer program. *Journal of Hydrology* **420-421**: 142–158.

Guggenmos MR, Daughney CJ, Jackson BM, Morgenstern U. 2011. Regional-scale identification of groundwater-surface water interaction using hydrochemistry and multivariate statistical methods, Wairarapa Valley, New Zealand. *Hydrology and Earth Systems Science Discussion* **8**: 6443–6487 DOI: 10.5194/hessd-8-6443-2011.

Hart DR, Mulholland PJ, Marzolf ER, DeAngelis DL, Hendricks SP. 1999. Relationships between hydraulic parameters in a small stream under varying flow and seasonal conditions. *Hydrological Processes* **13**: 1497–1510.

Harvey JW, Bencala KE. 1993. The effect of streambed topography on surface-subsurface water interactions in mountain catchments. *Water Resources Research* **29**: 89–98.

Harvey JW, Wagner BJ. 2000. Quantifying hydrologic interactions between streams and their subsurface hyporheic zones. In *Streams and Ground Waters*, Jones JB, Mulholland PJ (eds). Academic Press: San Diego, CA; 4–41.

Harvey JW, Wagner BJ, Bencala KE. 1996. Evaluating the reliability of the stream tracer approach to characterize stream-subsurface water exchange. *Water Resources Research* **32**: 2441–2451.

Hatch CE, Fisher AT, Revenaugh JS, Constantz J, Ruehl C. 2006. Quantifying surface water-groundwater interactions using time series analysis of streambed thermal records: method development. *Water Resources Research* **42**: W10410.

Hayashi M, Rosenberry DO. 2002. Effects of ground water exchange on the hydrology and ecology of surface water. *Ground Water* **40**: 309–316.

Hester ET, Doyle MW. 2008. In-stream geomorphic structures as drivers of hyporheic exchange. *Water Resources Research* **44**: W03417.

Hinton MJ, Schiff SL, English MC. 1997. The significant of storms for the concentration and export of dissolved organic carbon from two Precambrian Shield catchments. *Biogeochemistry* **36**: 67–88.

Inamdar SP, Christopher SF, Mitchell MJ. 2004. Export mechanisms for dissolved organic carbon and nitrate during summer storm events in a glaciated forested catchment in New York, USA. *Hydrological Processes* **18**: 2651–2661.

Kasahara T, Hill AR. 2006. Hyporheic exchange flows induced by constructed riffles and steps in lowland streams in southern Ontario, Canada. *Hydrological Processes* **20**: 4287–4305.

Kasahara T, Wondzell SM. 2003. Geomorphic controls on hyporheic exchange flow in mountain streams. *Water Resources Research* **39**: 1005. DOI: 10.1029/2002WR001386.

Lautz LK, Fanelli RM. 2008. Seasonal biogeochemical hotspots in the streambed around restoration structures. *Biogeochemistry* DOI: 10.1007/s10533-008-9235-2

Lautz LK, Ribaudo RE. 2012. Scaling up point-in-space heat tracing of seepage flux using bed temperatures as a quantitative proxy. *Hydrogeology Journal* **20**:1223–1238. DOI: 10.1007/s10040-012-0870-2

Lewandowski J, Lischeid G, Nutzmann G. 2009. Drivers of water level fluctuations and hydrological exchange between groundwater and surface water at the lowland River Spree (Germany): field study and statistical Analyses. *Hydrological Processes* **23**: 2117–2128. DOI: 10.1002/hyp.7277

Malcolm IA, Soulsby C, Youngson AF, Hannah DM, McLaren IS, Thorne A. 2004. Hydrological influences on hyporheic water quality: implications for salmon egg survival. *Hydrological Processes* DOI: 10.1002/hyp.140.5.

Malcolm IA, Soulsby C, Youngson AF. 2006. High frequency logging technologies reveal state-dependent hyporheic process dynamics: implications for hydroecological studies. *Hydrological Processes* DOI: 10.1002/hyp.6107.

Morrice JA, Valett HM, Dahm CN, Campana ME. 1997. Alluvial characteristics, groundwater-surface water exchange and hydrologic retention in headwater streams. *Hydrological Processes* **11**: 253–267.

Sawyer AH, Cardenas MB, Bomar A, Mackey M. 2009. Impact of dam operations on hyporheic exchange in the riparian zone of a regulated river. *Hydrological Processes* **23**: 2129–2137.

Shibata H, Sugawara O, Toyoshima H, Wondzell SM, Nakamura F, Kasahara T, Swanson FJ, Sasa K. 2004. Nitrogen dynamics in the hyporheic zone of a forested stream during a small storm, Hokkaido, Japan. *Biogeochemistry* **69**: 83–104.

Storey RG, Howard KWF, Williams DD. 2003. Factors controlling riffle-scale hyporheic exchange flows and their seasonal changes in a gaining stream: a three-dimensional groundwater flow model. *Water Resources Research* **39**: 1034. DOI: 10.1029/2002WR001367

Valett HM, Fisher SG, Grimm NB, Camill P. 1994. Vertical hydrologic exchange and ecological stability of a desert stream ecosystem. *Ecology* **75**: 548–560.

Westhoff MC, Bogaard TA, Savenije HHG. 2011. Quantifying spatial and temporal discharge dynamics of an event in a first order stream, using distributed temperature sensing. *Hydrology and Earth Systems Science* **15**: 1945–1957.

Wondzell SM. 2011. The role of the hyporheic zone across stream networks. *Hydrological Processes* **25**: 3525–3532.

Wondzell SM, Swanson FJ. 1996. Seasonal and storm dynamics of the hyporheic zone of a 4th-order mountain stream. *Journal of the North American Benthological Society* **15**: 3–19.

Wroblicky GJ, Campana ME, Valett HM, Dahm CN. 1998. Seasonal variation in surface-subsurface water exchange and lateral hyporheic area of two stream-aquifer systems. *Water Resources Research* **34**: 317–328.

Zarnetske JP, Haggerty R, Wondzell SM, Baker MA. 2011. Dynamics of nitrate production and removal as a function of residence time in the hyporheic zone. *Journal of Geophysical Research*. DOI: 10.1029/2010JG001356

